Geofísica Internacional (2019) 58-4: 279-293

Original paper

Electrical Resistivity Tomography for the detection of subsurface cavities and related hazards caused by underground coal mining in Coahuila

José A. Batista Rodríguez*, Marco A. Pérez Flores, Yuri Almaguer Carmenates and Maximiliano Bautista Hernández

Received: September 05, 2018; accepted: September 27, 2019; published on line: October 01, 2019

Resumen

En este estudio se utilizó Tomografía de Resistividad Eléctrica para identificar cavidades en el subsuelo de la región carbonífera del Estado de Coahuila, originadas por la minería del carbón, y con ello se valora el riesgo geológico inducido. Las mediciones se tomaron a lo largo de perfiles ubicados en las proximidades de carreteras y puentes, dentro de sectores de actividad minera. Estos perfiles se ubican evitando las propiedades privadas y abarcando algunas zonas de hundimientos de las carreteras. Se considera que la subsidencia es antropogénica y está relacionada con la actividad minera somera y relativamente profunda. En las secciones transversales de resistividad eléctrica obtenidas del proceso de inversión se identifican varias cavidades con diferentes formas desde los 7 m de profundidad. La mayoría de estas estructuras causan deformaciones en la superficie, generando hundimientos y fracturas en las carreteras. De forma general, las cavidades identificadas en dos de los sectores analizados se encuentran rellena de agua o sedimentos. En un tercer sector todas las cavidades están vacías o parcialmente rellenas con material colapsado de sus paredes y techos. Las secciones eléctricas revelan otras características del ambiente geológico, tales como zonas de disminución de los niveles acuíferos, inclinación de estratos (que indican paleo-subsidencia del terreno), fallas y fracturas que afectan la secuencia estratigráfica. La disminución de los niveles de los acuíferos indica cambios en el régimen hidrodinámico de las aguas subterráneas que han sido ocasionados por los espacios vacíos generados por la minería. Estos cambios provocan que el subsuelo se hunda debido a la presión litostática y el peso de los vehículos que pasan por encima de las carreteras. Como resultado final, se ubican en los tres sectores analizados, las áreas con mayor riesgo potencial de peligros relacionados con el hundimiento del subsuelo.

Palabras clave: minería subterránea del carbón, cavidades, subsidencia, Tomografía de Resistividad Eléctrica, región carbonífera de Coahuila.

J. A. Batista Rodríguez*
Y. Almaguer Carmenates
M. Bautista Hernández
Escuela Superior de Ingeniería
Universidad Autónoma de Coahuila
Nueva Rosita, 26830, México
*Corresponding author: josebatista@uadec.edu.mx

M. A. Pérez Flores
División de Ciencias de la Tierra, CICESE
Baja California, 22860, México

Abstract

This study used Electrical Resistivity Tomography (ERT) to identify the subsurface cavities in the carboniferous region on the State of Coahuila caused by underground coal mining and the hazards they induce. Measurements were taken next to roads and bridges support in three sectors with mining activity. Authors used roads to run the ERT profiles in order to avoid private properties, with some of these profiles including areas with subsidence. It is considered that subsidence is an anthropogenic related to both shallow and relatively deep underground mining activity. The electrical resistivity cross-sections obtained from the geophysical inversion process identified several cavities with a variety of dimensions ranging upwards from a depth of 7 m. Most of these structures cause deformations on surface in the form of subsidence or fractures. In general, the cavities identified in two of the sectors analyzed are filled with water or sediments. In a third sector analyzed in this study, all cavities were either empty or partially filled with collapsed material from their walls and ceiling. Geo-electrical sections reveal other characteristics of the geological environment, such as zones in which aquifer levels decrease, strata dipping (indicating prior subsidence), and faults and fractures that affect the stratigraphic sequence. The decrease in aquifer levels indicates changes in the hydrodynamic groundwater regime that have been caused by the voids generated by mining. These changes cause the ground to sink due to lithostatic pressure and the weight of the vehicles passing above. As a final result, the areas at the greatest potential risk of hazards related to ground subsidence are located within the three analyzed sectors.

Key words: underground coal mining, cavities, subsidence, Electrical Resistivity Tomography, the carboniferous region of Coahuila.

Introduction

The mining industry has been well known for the potential of risk it generates, mainly underground mining operations. These operations can generate geotechnical accident, such as, roof collapse, subsidence, landslides, rock burst, etc., which negatively affects economic profitability. Underground mining operations generating damage on the surface of the ground in urbanized and populated zones. The most important and most frequent problems related to mining operation include mine subsidence and risk to buildings, for example, in the Upper Silesia Coal Basin (Strozik *et al.*, 2016) and in some coal mining of China (Chugh, 2018).

The Sabinas basin, located in Northeastern Mexico, contains significant coal deposits (Figure 1) distributed across eight sub-basins (Rivera-Martínez and Alcocer-Valdés, 2003). The exploitation of this mineral resource through open pit and underground mining (mainly longwall mining method) has caused major modifications to the environment, including the generation of underground galleries and low relief areas. When caused by rudimentary mining, these galleries can be very shallow and small, whereas those caused by deep mining (conducted at approximately 350 m) may be much larger (SE, 2017). These galleries can often collapse, causing deformations to the geological environment such as fractures, faults, and terrain collapse (Bruhn *et al*., 1978). In areas with shallower galleries, there is a greater hazard of subsidence (Bruhn *et al*., 1978; Peng, 2008), a process which has been identified in some sectors of the Sabinas basin (Serrano-González, 2014) and which affects socio-economic infrastructure such as roads, buildings, and bridges supports. The locations of these sectors suggest that this process could be related to collapsing of underground galleries, namely subsurface cavities generated by underground coal mining.

Cavities generated by underground coal mining can be partially or completely air-filled, water-filled or sediment-filled (Van Schoor, 2002; Zhou *et al*., 2002). In all cases, the cavities can be identified by the contrast between their physical properties and the surrounding geological environment. Electrical resistivity is one of the main physical properties that enable the characterization of these structures (Militzer *et al*., 1979; Putiska *et al*., 2012).

In the study region, coal is located in a sedimentary sequence formed by sandstones and shales overlapped by conglomerates or sediments such as alluviums, sands and clays (SGM, 2003; Corona-Esquivel *et al*., 2006; González-Sánchez *et al*., 2007).

In this research, the ERT was used in three sectors of the Sabinas coal basin to locate and characterize subsurface cavities related to underground coal mining and identify

the anthropogenic hazard they induce. The three sectors selected are located in areas in which mining activity is undertaken next to roads, bridges and buildings. Two sectors with subsidence and one without visible subsidence were selected. The subsidence in one of the sectors was related to shallow mining while it was related to relatively deep mining in the other.

Geological setting

The Sabinas Basin initially developed on the margin of the North American Craton during the opening of the Gulf of Mexico in the early Mesozoic. This basin is a depression formed by a series of subsided blocks. The Sabinas Basin is separated from the Chihuahua Basin by blocks elevated to the Northwest (Eguiluz de Antuñano, 2001). It developed over several evolutionary phases, with the first phase comprising a long period of Triassic-Lower Jurassic magmatic-arc activity. A rupture of the lithosphere occurred in the second phase, while the rift, associated with the opening of the Gulf of Mexico, developed in the third phase (Eguiluz de Antuñano, 2001).

Evaporite, carbonate and detrital formations predominate in the lower basin levels, whereas detrital formations predominate in the upper levels, such as in the San Miguel and Olmos Formations. The Olmos Formation is of great significance because it presents the most exploitable coal seams found in the region (Eguiluz de Antuñano, 2001; Corona-Esquivel *et al*., 2006; González-Sánchez *et al*., 2007). In the study area, the San Miguel and Olmos Formations outcrop, as well as Sabinas Conglomerate and alluvial sediments (SGM, 2003; Figure 1).

The coal deposits are distributed across eight sub-basins (Rivera-Martínez and Alcocer-Valdés, 2003; Figure 1). The most significant because of its extensive size and coal content, the Sabinas sub-basin is the most explored and exploited, containing at least three coal beds, which have been found at depths up to 350 m (SE, 2017).

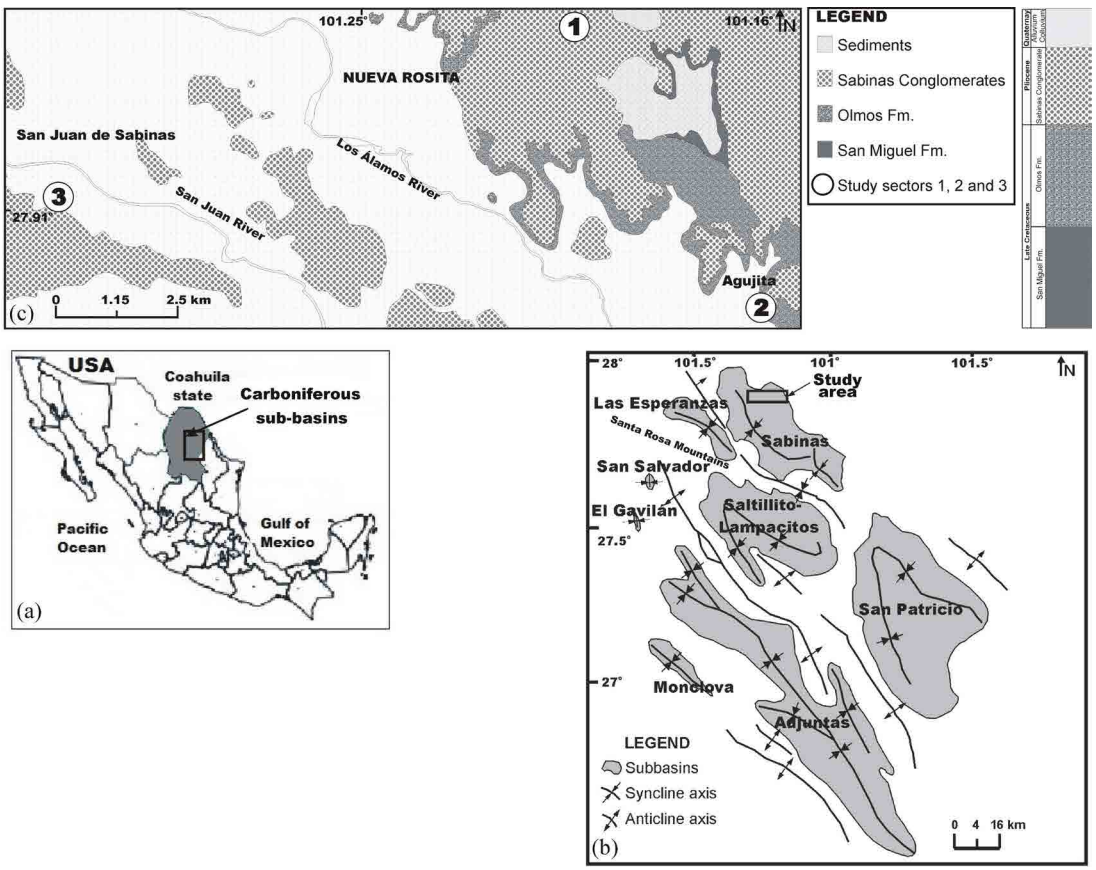

Figure 1. a) Location of carboniferous sub-basins in Northeastern Mexico. b) Carboniferous sub-basins in Northeastern Mexico (modified from Rivera-Martínez and Alcocer-Valdés, 2003). Rectangle indicates location of the study area. c) Geological map of the study area. Original scale 1:50,000 (modified from SGM, 2003). 1, 2 and 3 indicate study sectors.

Coal mining in the Sabinas basin

As mentioned previously, two ways of extracting coal are used in the Sabinas basin, surface and underground mining. The surface mining is carried out as opencast (open pit) mining, mainly. This type of mining is used when the coal outcrops or is located a few meters deep; approximately 20 m (Figures 2a and 2b). In this basin most of the coal is extracted using underground mining with the longwall mining method considering the depths and a tilt of the coal beds. With this mining method the area to be mined is divided into a series of elongate panels accessed from an entry roadway (Figure 3a). In this case, the hydraulic and self-supporting pillars temporarily maintain the roof, while the coal is extracted; later this roof can collapse (Thomas, 2013). The vertical shaft is another method of entry for underground mines (Figure 3b). During the underground mining, when the coal seam is excavated, the vertical stresses above it are generated and they can cause the overburden fails completely and it is transferred to the goaf, generating a subsequent surface subsidence (Figure 4; Van der Merwe and Madden, 2010).

Hydrogeological setting

Two aquifers systems are recognized in the Coahuila coal mining region (CONAGUA, 2015). First system is found in the Early Cretaceous limestones, mainly in the Cupido and Aurora formations located to the southeast of the Santa Rosa Mountains of Coahuila. Several water wells indicate that this aquifer system is the deepest (about 800 m). This aquifer is classified as mainly confined, although there are some sites where limestones outcrop and the aquifer becomes free-type (e.g., Santa Rosa Mountains; Figure 1). The permeability of this aquifer system is related to fractures and the chemical dissolution of rocks.

Second system is formed by shallow aquifers mainly located in Quaternary alluviums and in Sabinas Conglomerates (Pliocene) with a static level from 5 to 15 m. This system includes fractures and weathering zones within the conglomerates and the detrital formation in the upper levels of the Late Cretaceous. Located in granular materials (alluviums and conglomerates), these aquifers are classified as free-type, and semi-confined-type in the Late Cretaceous rocks. Aquifers in the granular materials may seep down through fractures into the Upper Cretaceous Formations (e.g. the Escondido, Olmos, San Miguel, Upson, Austin and Eagle Ford formations, as well as the Washita Group). The Olmos Formation is considered an aquitard because it stores fluids with low permeability (CONAGUA, 2015).

The second aquifer system is of great significance to the study of the cavities generated by mining activity, because some coal seams in the Olmos Formation are located below the static level (Figure 2b), which indicates flooding of the underground galleries.

Data acquisition and processing

Electrical Resistivity Tomography (ERT) data was collected along ten different profiles in areas that have been affected by underground galleries (cavities) in the carboniferous region of Coahuila (Table 1). In order to locate cavities situated under roads, two profiles were set parallel each other and on the roads, close to the principal buildings in order to ascertain infrastructure damage (Figures 5, 6 and 7).

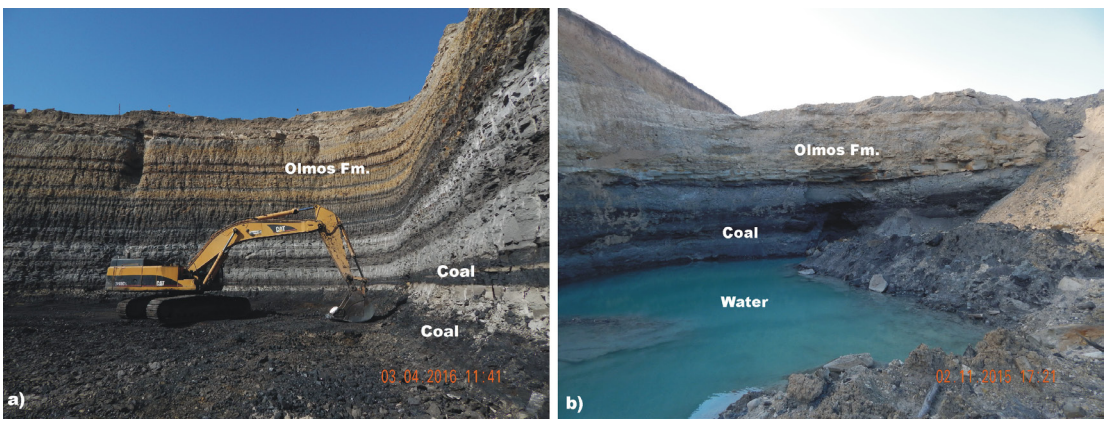

Figure 2. Coal open pit mines in Sabinas basin. a) Coal seams in the Olmos Fm. b) Aquifer cutting coal seams in the Olmos Fm.

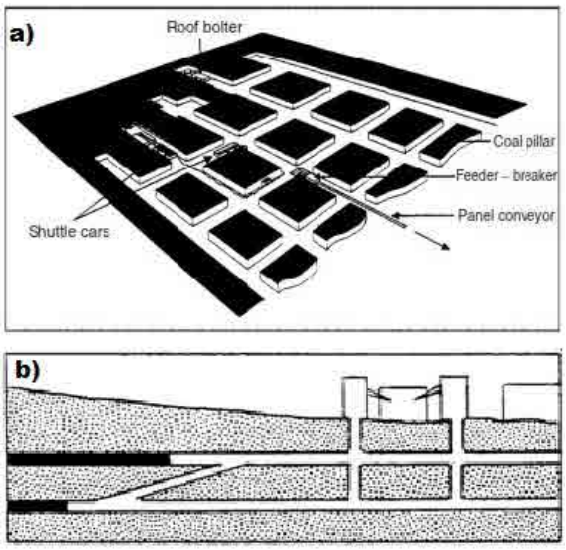

Figure 3. a) Method of mining in underground mine: room and pillar mining (Hunt and Bigby, 1999). b) Method of entry for underground mine: vertical shafts (Ward, 1984).

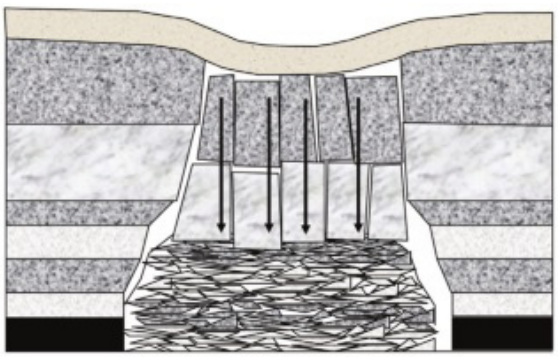

Figure 4. An failed overburden and its load transferred to the goaf. The abutments are stress relieved (Van der Merwe and Madden, 2010).

Table 1. Characteristics of ERT data acquisition. Equipment: AGI SuperSting R1/IP/SP with schlumberger, wenner and dipole-dipole arrays in all profiles. All measurements were carried out with two cycles, maximum current of 2000 mA and measure time of 1.2 s.

Sector	Profile	Length (m)	Spacing of electrode (m)
1	1 (P1)	270	10
	2 (P2)	270	10
	3 (P3)	540	20
	4 (P4)	400	20
2	1 (T1)	270	10
	2 (T2)	270	10
	3 (T3)	270	10
3	1 (G1)	270	10
	2 (G2)	960	20
	3 (G3)	540	20

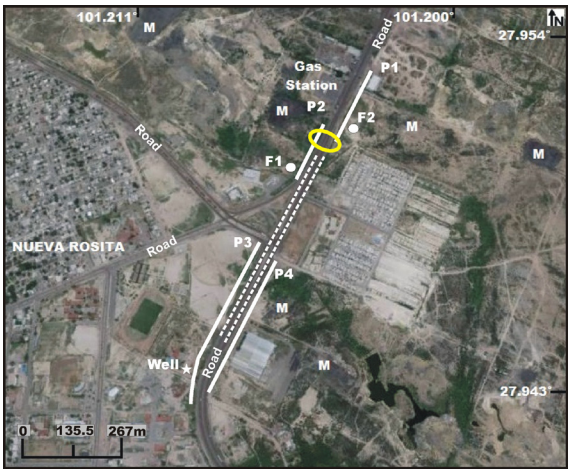

Figure 5. Study Sector 1. M indicates mining zones. Continuous black lines indicate location of the measurement profile (P1, P2, P3 and P4). Dashed black lines indicate location of the bridge. F1 and F2 indicate the reference point for the photographs shown in figures 9b and 9c. Yellow ellipse indicates a subsidence zone on the road (view photography in Figure 9a). Star indicates well.

Figure 6. Study Sector 2. Continuous white lines indicate location of the measurement profile (T1, T2 and T3). F1 and F2 indicate the reference point for the photographs shown in figures 13a and 13b.

The AGI SuperSting R1/IP/SP was used for data collection (Figure 8) using schlumberger, wenner and dipole-dipole arrays (with 10 m and 20 m electrode spacing), which are the most common arrays used in electrical resistivity tomography.

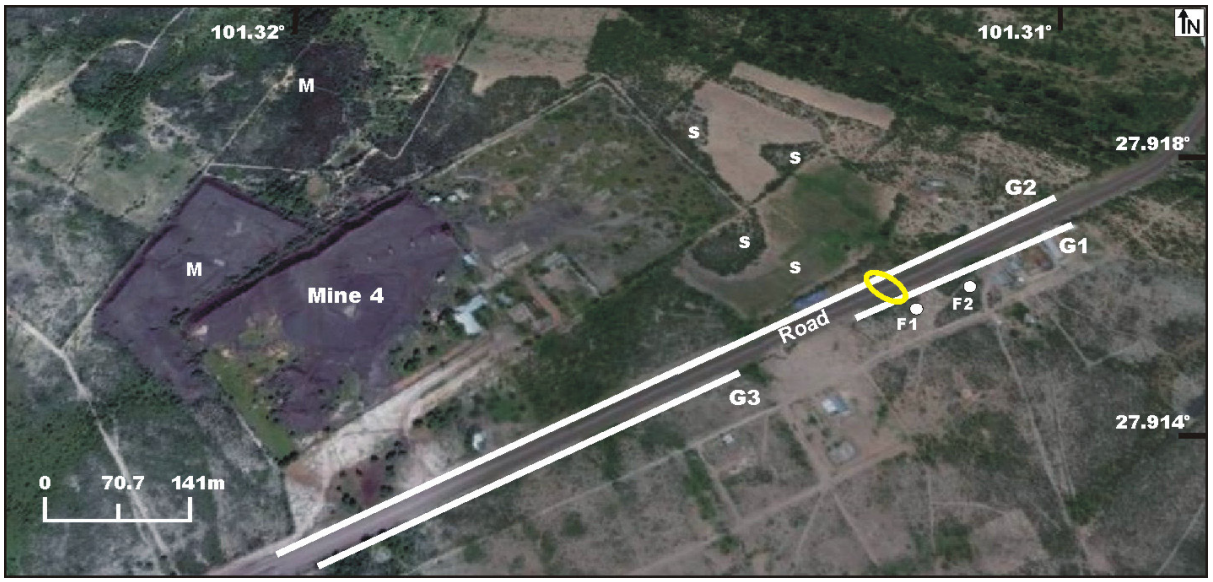

Figure 7. Study Sector 3. Continuous white lines indicate location of the measurement profile (G1, G2 and G3). S indicates areas with a sinkhole. F1 and F2 indicate the reference point for the photographs shown in figures 14c and 14d. Yellow ellipse indicates a subsidence zone on the road (view photography in Figure 14a).

Figure 8. Data collection using the AGI SuperSting R1/IP/SP.

Each ERT array has a specific underground current pattern and it give us a specific apparent resistivity pseudo-section. That means that each ERT array looks the subsurface electrical structures in different way according their currents pattern. When doing the geophysical inversion of a single ERT array, we obtain the estimated underground true resistivity since the point of view of that specific currents pattern. If we try three different ERT arrays, we will have three slightly different versions of the underground according the current patterns of every array. If we do joint inversion of the three arrays, we impose the geophysical inversion that a single model must explain the three data sets. Meaning that the more arrays we use, the better underground model we will obtain (less uncertainty). Because, we are using many currents patterns or many points of view for a single underground reality.

An overlap on the data profiles was created between the lines in P2 on Sector 3 (Figure 7) in order to ensure the continuity of the model and attain a length greater than 540 m. This overlap was achieved using the Roll-along technique, in which the electrode cable advance forward along the measurements profile by moving your cable sections in a leap-frog way. Subsequently, the joint inversion of the three arrays was performed using EarthImager 2D resistivity inversion software developed by Advanced Geosciences, Inc. The software uses a finite element algorithm to compute the estimated real resistivity (model) thought the apparent resistivity data (AGI, 2009), from which a geological explanation for every 2D resistivity model was found (Huebner and Thornton, 1995). The geophysical inversion gives us the resistivity model with a very low or the lowest Root Mean Square (RMS) error value, according the imposed inversion parameters. This RMS error quantifies the difference between the apparent resistivity measured in the field and the apparent resistivity obtained from the response of the 2D resistivity model estimated. In this way, a single resistivity model was obtained for every profile with three datasets (schlumberger, wenner and dipole-dipole).

Results

In order to evaluate how underground coal mining has affected and how it may affect in the future the socio-economic infrastructures (e.g. roads, buildings, bridges, etc.) located within the Sabinas Basin, three study sectors were selected for the measurement of the ERTs. Sectors 1 and 2 were located in a very shallow underground mining area. The first sector has subsidence on the road surface. The third sector was located in a relatively deep underground mining area in which subsidence on the road was also present.

The interpretation of the ERT results aimed; to locate cavities, to show the characteristics of the geological environment that are related to the observed subsidence on the road surface and to guess the probability that this process occurs in the future.

For every profile the water table was obtained from using static level from CONAGUA (2015) of 5 to 15 m, as well as the resistivity values in each ERT.

Sector 1

This sector contains both a road and a bridge support (Figure 5), with subsidence found on the road at the northeast end (Figure 9a), which could be related to the underground coal mining (Peng, 2008) due the shallower mining activities in this sector and its surroundings.

In order to locate and characterize the subsidence-related hazard zones, four ERT profiles (referred as P1, P2, P3 and P4) measured on both sides of the road and at the beginning of the bridge support (Figure 5). The profiles ran on a NE-SW direction of the sector, covering the areas of the road affected by subsidence (profiles 1 and 2, with lengths of 270 m) and other areas where this geological process is not observed (profiles 3 and 4). Conglomerates were found to outcrop in the four profiles (Figures 1, 10 and 11).

The northeastern end of Profile 2 covers the area of the road where subsidence is found (Figure 9a). Two possible cavities are identified with the ERT below the road, at 13 m depth, with both structures presenting different electrical resistivity, size and depth (Figure 10). It can be inferred from the resistivity image that the first cavity is smaller, larger resistivity and partially empty or filled with dry sediments. The second cavity is larger, lower resistivity and filled with either water or water-saturated sediments (Van Schoor, 2002; Zhou *et al*., 2002; Martínez-López *et al*., 2007; Putiska *et al*., 2012). Above these cavities, around 7 m depth, a small size aquifer is located within the Sabinas Conglomerates (CONAGUA, 2015). Above the area that covers both cavities, the road is highly fractured, with some fractures cutting across the entire road (Figures 9b and 9c). The electrical tomography suggests that some of these fractures penetrate into the subsoil, mainly in the area of the second cavity (see the inferred fracture in Figure 10).

Four small cavities are found in the SW end of Profile 2 (Figure 10), located next to the bridge (Figure 5) with subsidence on the road (Figure 9). Two cavities have very low resistivity, while the other two are more resistive, smaller and shallower (approximately 7 m). The cavity found at the center of the profile is clearly the cause of fracturing on the road surface. Moreover, in this zone, the ERT results show at patterns that suggest subsidence, namely, zones of low resistivity (represented by the light gray color) with a convex form (Figure 10).

Profile 1 also shows several cavities from a depth of 7 m onwards, most of which present low values of resistivity and are small in size. Above these cavities water table of about 5 m inside the conglomerates is located. According to the ERT, the geometry of these structures shows patterns of probable subsidence, although no visible deformations are observed on the surface of the roads. These patterns were found in the ERT results for zones with low resistivity and convex shapes with respect to the surface (Figure 10). These zones resemble the characteristic descent into a small basin which is caused by the accumulation of sediments. Towards the northeast of the profile, a large cavity with very low resistivity was observed, extending from a depth of 10 to 50 m (x=110 m). Above this cavity, the road presented no subsidence; however, the ERT showed that it is so close to surface that we expect possible fracturing on surface. We found, in some buildings adjacent to the road fractured walls. All fracture systems observed on the road are perpendicular and oblique to the highway (Figures 9b and 9c), following the probable galleries direction (Peng, 2008). The fracture systems follow three different directions: perpendicular to the road on a NW-SE direction; oblique on a NE-SW direction; and, a NW-SE direction.

While profiles 1 and 2 run paralleled on both road sidewalks, but they have an offset each other (Figure 5). They only coincide until x= 60 m in P2 (Figure 10). For this reason, it is not possible to assess whether the cavities continue on another sidewalks.

Figure 9. Sector 1. a) Image showing the subsidence of the road. b) and c) Image showing fractures on the road surface in profile P2. Arrows indicate location and direction of the fractures. Reference points for the photographs shown in b) and c) are indicated as F1 and F2 in Figure 2, respectively. F1 and F2 also are indicated in Figure 9a.

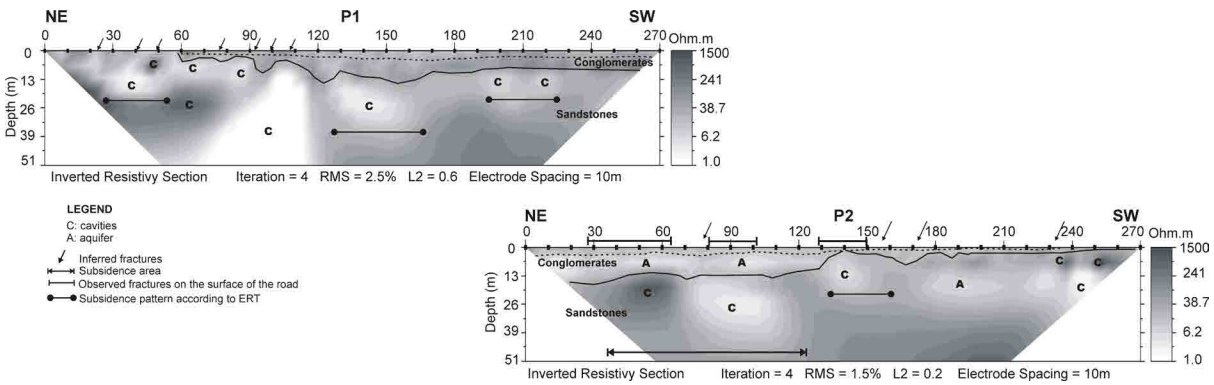

Figure 10. ERT of Sector 1 (profiles P1 and P2). The section of P2 from 170 to 270 m is located next to the bridge. Continuous curved lines indicate boundaries between rocks and discontinuous curved lines indicate water table. The profiles are located graphically according to their position in the field (see Figure 5).

The bridge support is found at the southwest end of the sector, where profiles 3 and 4 were measured (Figure 5) as having lengths of 540 m and 400 m, respectively and their resistivity models are shown in Figure 11. In this zone, the road presented no subsidence and no fractures; however, the ERT results indicate cavities patterns by underground mining activity. These patterns are circular and oval shape and they are located at two depth levels (approximately 22 m and 50 m). Some of these cavities were observed at both sidewalks, indicating that they are connected and cross under the road. All cavities identified are low resistivity (represented by the light gray color). Values lower than 10 ohm-m suggests that the cavity is water-filled (Van Schoor, 2002; Zhou *et al*., 2002; Martínez-López *et al*., 2007;

Putiska *et al*., 2012). This water is provided by the aquifers located in conglomerates and the upper level of the Olmos Fm. (Figure 11). The water table was determined with using a well located in the profile P3 (x=465 m) with a water table at 12 m. Their variations are stablished using resistivity values. Cavities with a resistivity between 30 and 200 ohm-m may be filled with sediments slightly saturated with water (represented by the light gray color; Van Schoor, 2002; Zhou *et al*., 2002; Martínez-López *et al*., 2007; Putiska *et al*., 2012), probably due to cavity collapse. It is possible that some faults or fractures infiltrated water inside the cavities as a first stage and the absence of water as a second stage could cause the collapse itself.

The larger cavities (30 m wide and 25 to 35 m high) identified at a depth larger than 30 m, do not produce visible road deformation; however, this is not a general rule. Some of the zones with probable land subsidence (x=360 m in P3 and x=180 in P4) are related to cavities deeper that the mentioned depth.

It should be noted that, most of the cavities identified are located on both sides of the bridge support. The bridge support itself is located in an area with a large hazard level.

These results suggest that special attention should be paid to both of these areas and to activate a system for monitoring the roads and the bridge integrity in order to avoid damage due the gradual or sudden land collapse.

Sector 2

A road without subsidence is located in this sector, in spite of being located in a zone with many evidences of shallow underground mining activity (Figure 6). ERT results were obtained for both sidewalks of this road. The three parallel profiles are referred as T1, T2 and T3 (Figure 6). Profiles T1 and T2 are on the same sidewalk but have and offset of 10 m, due the heavy truck traffic. While profiles T3 and T1 are parallel and on opposed sidewalks (Figure 6). The 2D resistivity models obtained are shown in Figure 12.

Sediments with a very low resistivity outcrop at the SE end of T1 and they extend to depths larger than 35 m (Figure 12). Electrical resistivity values suggest that these sediments are water saturated, in which the water table oscillates around 5 m, deepening to the NW of the profile T1, according to the resistivity values. Towards the SW end of the profile, conglomerates outcrop and extending to 14 m depth. Several cavities, beginning at a depth of 14 m, are identified in the sandstones underlying the sediments and conglomerates, all of which recorded low resistivity values (Figure 12), indicating that these structures are probably filled with water or water-saturated sediments.

This study identified several fracture systems on the road above the identified cavities (Figure 12), with most of these fractures running perpendicular to the road (Figures

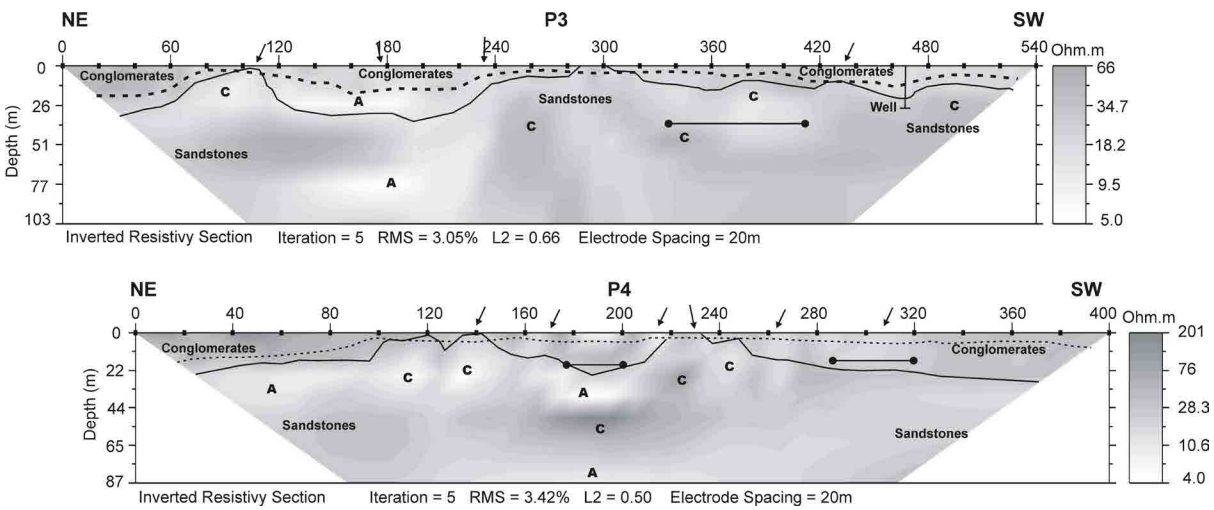

Figure 11. ERT of Sector 1 (P3 and P4). The profiles are located graphically according to their position in the field (see Figure 5). Continuous curved lines indicate boundaries between rocks and discontinuous curved lines indicate water table. The section of P3 from 0 to 280 m and the section of P4 from 0 to 230 m are located next to the bridge. Vertical line indicate well.

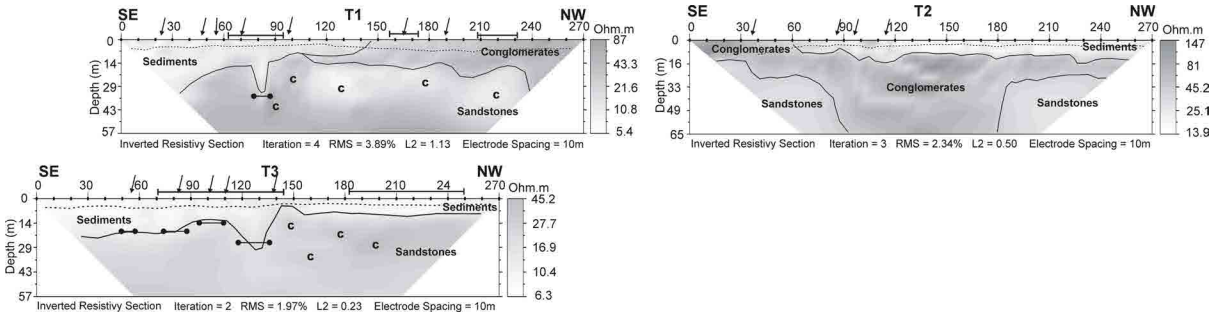

Figure 12. ERT of Sector 2. The profiles are located graphically according to their position in the field (see Figure 6). Continuous curved lines indicate boundaries between rocks and discontinuous curved lines indicate water table.

13a and 13b). The ERT models also present patterns that suggest deep extended fracture systems related to the cavities. Similarly, the ERT model for T1 shows a pattern of probable subsidence with low resistivity (represented by the light gray color) and a convex form, while on the road increases the density of fractures and decreases the spacing between them.

Sediments and conglomerates outcrop in the T1 and T2 models (Figure 12), while ten meters depth, conglomerates cover almost the entire Profile 2 (T2) and raise a thickness of 50 m at the center. No cavities in the central part are identified in the ERT model. This explains why no fractures were found on the road.

Profile 3 (T3) is located on the opposite sidewalk (Figure 12). Only sediments outcrop in Profile 3 and the cavities identified in Profile 1 also appear, suggesting that they are located below the road.

More road fractures were found on the east side than on the west (Figure 13b), which may be related to the outcrop of less competent materials (sediments) on the east side.

Sector 3

This sector includes a road which is located next to an abandoned underground coal mine (Mine 4 in Figure 7), which reached an approximate depth of 350 m. Two sections of extensive subsidence were identified on the road (Figure 14a), related, apparently, to underground mining.

In this sector, three ERTs were also obtained from profiles 1, 2 and 3, referred to here as G1, G2 and G3, respectively, with G1 measured at 270 m, G2 at 960 m, and G3 at 540 m. An overlap was implemented in G2 between the three segments of the line in order to ensure data continuity and, therefore, a 960 m-long continuous resistivity model. Several cavities were also identified in these profiles, most of them larger and deeper than those identified in the previously described sectors (Figure 15). Generally, cavities were identified at a depth of 30 m and reached up to 50 m in diameter.

Conglomerates outcrop the profiles measured in this study, while the ERT results reveal an aquifer (CONAGUA, 2015) attached to the sandstone contact. This aquifer is thicker and wider in lateral extension than those identified in the previous sectors (sectors 1 and 2). Resistivity values indicate that this aquifer has a very variable water table that can exceed 15 of static level reported by CONAGUA (2015). The results of this study permit the inference that cavities can be found at a depth of below 28 m.

Figure 15 shows that, generally, the aquifer level becomes deeper in the zones between the cavities (x=60 m, x=150 m and x=200 m in G1; x=200 m, x=290 m and x=440 m in G2; and, x=300 m in G3). Two of these zones are located just below the subsidence observed on the road (Figure 14a). One zone is located at the SW of G1 and another at around x=200 m in G2, while a third is found at around x=800 m at the SW end of G2 and at 380 m in G3 (Figure 15). In all the zones located between the cavities identified in this study, a high number of fractures were observed on the road (Figures 14b and 15).

Within the sandstones, another aquifer was found at a depth of 100 m below the cavities (Figure 15), in some areas connected to the upper aquifer located at x=200 m, x=460 m, and x=860 m in G2. This finding concurs with the CONAGUA (2015) results, which indicate the connection, through fractures, between the shallow and deep aquifers. These ERT

findings indicate a high level of fracturing at depth, which was also identified on the road surface (Figures 14c and 14d). The two zones presenting subsidence on the road surface are located at x=200 m and x=860 m in G2.

Most of the cavities identified in this study present high values of electrical resistivity, indicating that they are not water-filled and, instead air-filled or partially filled with sedimentary materials (Martínez-López *et al*., 2007; Putiska *et al*., 2012). These materials may be associated with the ceiling collapses that have occurred in the mining structures.

Discussions

Analysis of the ERT 2D models of the profiles measured in this study reveals several cavities, some located below the roads. The resistivity values in those structures suggest that they may either be empty or filled with water sediments. The road surface located above some of the cavities (sectors 1 and 2) presents a fracture system, apparently induced by the soil instability found around the cavities (Peng, 2008). Similarly, these fractures may also cause cavities to fill with water and wet sediments. The movement of groundwater into the cavities, the empty space of the cavities themselves or their collapse can cause geometrical deformation and the sinking of the land. This process is accelerated on the road surface due to the lithostatic pressure exerted on the cavities by the weight and vibration of the vehicles that circulate on the roads above on a daily basis.

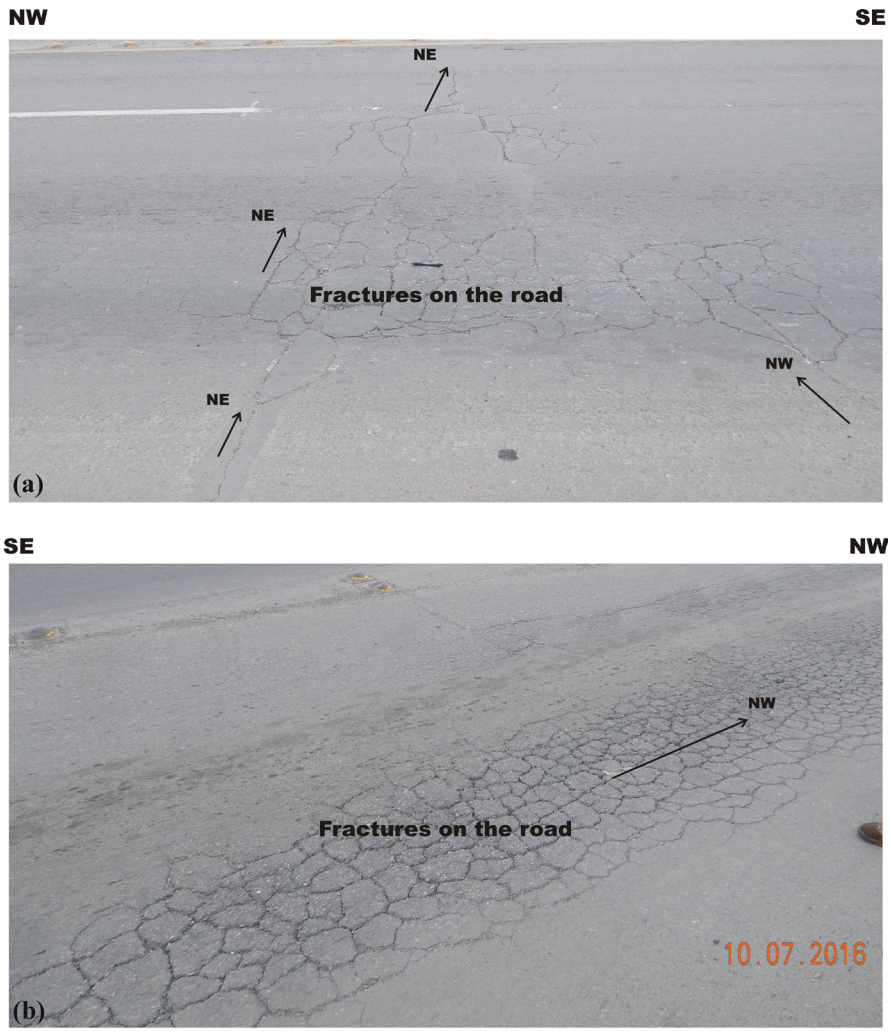

Figure 13. Images of fractures with signs of subsidence on the road surface in Sector 2. a) Profile T1. b) Profile T3. Arrows indicate location and direction of the fractures. Reference points for the photographs shown in a) and b) are indicated as F1 and F2 in Figure 6, respectively.

Cavity flooding can change the hydrodynamic groundwater regime, deepening the water table and modifying its natural flow. This can cause a loss of pore pressure in granular materials (e.g., alluviums and conglomerates) and generate land subsidence (Galloway and Burbey, 2011). Changes in the hydrodynamic groundwater regime not only disrupt the infrastructure (e.g., roads and bridges) but can also affect economic activities that depend on the use of water, as with livestock and agriculture.

Considering that road repairs have been carried out in some of the study sectors and, perhaps, due to land subsidence, it is possible that some of the subsided zones indicated by the ERT results, namely, zones of low resistivity (represented by the light gray color) and convex in form, have been previously filled with construction materials. For this reason, the evidence of sinking was erased, meaning that these areas can be considered areas of old subsidence.

Analysis of the ERT models for the 3 sectors shows some areas where no surface subsidence is present even when a cavity is located below. In these cases, it is possible that the relationships between the dimensions, depths and characteristics of the rocks (some which may be more competent than others) have not permitted subsidence to occur on the road surface. However, this study found various fracture systems directly related to these cavities on the most of the road surfaces examined. These fracture systems run in a transverse direction to the roads and, sometimes, completely cross them, for which reason, they were used as an indicator of a sinking process caused by underground coal mining (Bruhn *et al*., 1978; Peng, 2008). There is the possibility of an increase in these deformations over time, due to the weakening in the geological structures below the roads, as caused by the constant movement of vehicles above.

The subsidence patterns observed in Sector 3 are different from those found in sectors 1 and 2, in that, in Sector 3, the subsidence on the road surface occurs between two identified cavities rather than above them, as found in sectors 1 and 2. According to the ERT models generated for Section 3, the sinking seems to be related to the deepening of the aquifer level between two cavities. The cavities observed in Sector 3 are generally larger and deeper. Therefore, it is assumed that the fracture systems and subsidence patterns are related to the change in the hydrodynamic groundwater regime, probably caused by the water flow toward the underground galleries which is generated by deeper-level underground mining activities (occurring after 350 m). Once the underground cavities have been created, the underground water inside them is displaced, deepening the phreatic level. The conglomerates undergo a compaction process over time, leading to subsidence. At the NE end of Sector 3 (Figure 7), several sinkholes are observed (Figure 14b), indicating the existence of underground cavities generated by mining.

Figure 14. Sector 3. a) Image showing the subsidence of the road. b) Image of a sinkhole next to the road. c) and d) Images of fractures on the road surface in Profile P1. Reference points for the photographs shown in c) and d) are indicated as F1 and F2 in Figure 7, respectively.

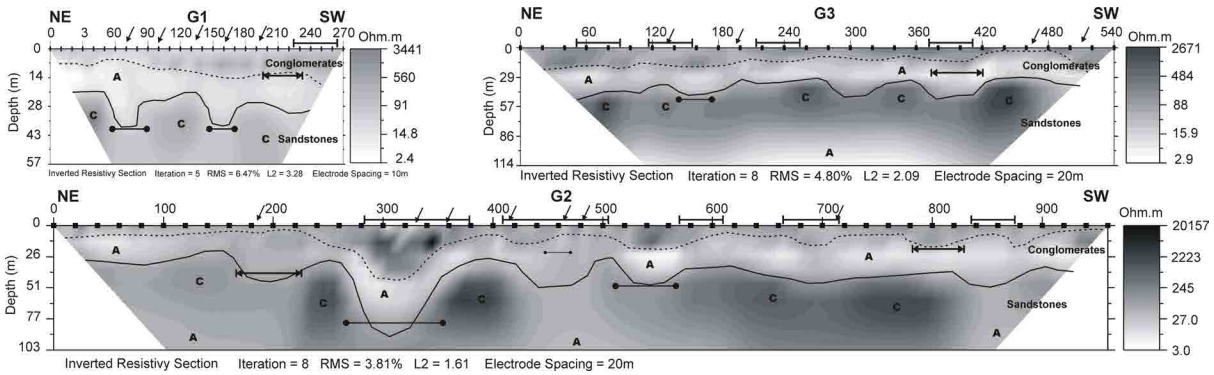

Figure 15. ERT of Sector 3. The profiles are located graphically according to their position in the field (see Figure 7). Continuous curved lines indicate boundaries between rocks and discontinuous curved lines indicate water table.

The fracture systems on the road surface in Sector 3 are found above the depressed zones identified, indicating the relationship between the two processes. The cavities present high resistivity values, indicating that they were not flooded by water from the upper level aquifer. The movement of groundwater can occur at lower levels, where cavities are larger and are related to the deepest mining activities (located at a depth of 350 m). According to CONAGUA (2015), the aquifers embedded in the granular materials of the Cenozoic (e.g., the Sabinas Conglomerates) may be connected through fracture systems with the Upper Cretaceous Formations (e.g., the Olmos Fm.).

The fracture systems observed on the road surface, the cavity patterns revealed by the ERT models in the three sectors, and the morphology of the aquifers suggest several potential hazard zones caused by the subsidence of the land in the study region.

According to the analysis carried out on the entire set of ERT resistivity models, there are several factors generating land subsidence due to the underground cavities. The main factors are: the size and depth of the cavity, the material with which it is filled or whether or not it is filled at all; the rock type and the level at which it fractures; and, the presence of an aquifer and their depth and thickness. When the cavities are empty, larger in size and not as deep, the hazard of subsidence increases, as it does if the cavity is located in rock that is non-competent and/or with a high propensity to fracture. Similarly, the presence of large aquifers above these cavities, combined with fractured or faulted rocks, will change the hydrodynamic groundwater regime and increase the hazard of subsidence.

Conclusions

Analysis of the ERT models applied to the three sectors from the northern end of the Sabinas Basin reveals cavities generated by underground coal mining. Some of these cavities have caused subsidence and a fracture system on the road surface, and damage to the surrounding buildings. These ERT models also show other characteristics of the geological environment caused by the fractures and the sinking of the roads, such as the decrease in the level of the aquifers, the fractures and faults that affect the stratigraphic sequence, and the layering of some strata (zones of low resistivity with a convex form) that show prior subsidence. According to the analysis carried out, the subsidence observed in Sector 1 is mainly related to very shallow cavities generated by shallow underground mining, whereas the subsidence in Sector 3 is related to the decrease in the level of the aquifers, as caused by changes in the hydrodynamic regime of the underground water, which is linked to deep-level mining activities. The distribution and characteristics of the cavities identified in the three sectors, as well as the geological characteristics inferred, suggest that the areas containing the profiles measured by this study are potentially hazardous. Fracture systems observed on the road surface without subsidence and located above the cavities identified via ERT are indicators of the initial stage of the deformation on the roads, as related to the process of subsidence.

Acknowledgments

We thank the University Autonomous of Coahuila and CICESE for its support of this research.

References

Advanced Geosciencies, Inc (AGI), 2009, Instruction Manual for EarthImager. Version 2.4.0. Resistivity and IP Inversion Software, 139 pp.

Bruhn, R.W., Magnuson, M.O., Gray, R.E., 1978, Subsidence over the mined-out Pittsburgh Coal. A.S.C.E. Convention ´Coal Mine Subsidence´ session, Pittsburgh, Pa, USA, April, pp. 26-55.

Comisión Nacional del Agua (CONAGUA), 2015, Actualización de la disponibilidad de media anual de agua en el Acuífero Región Carbonífera (0512), Estado de Coahuila. 27 pp. https://www.gob.mx/cms/uploads/attachment/file/102852/DR_0512.pdf. 06-10-2016.

Corona-Esquivel, R., Tritlla, J., Benavides-Muñoz, M.E., Piedad-Sánchez, N., Ferrusquía-Villafranca, I., 2006, Geología, estructura y composición de los principales yacimientos de carbón en México. *Boletín de la Sociedad Geológica Mexicana*, 57, 141-160.

Chugh, Y.P., 2018, Concurrent mining and reclamation for underground coal mining subsidence impacts in China. *International Journal of Coal Science & Technology*, 5(1), 18-35.

Galloway, D.L., Burbey, T.J., 2011, Review: regional land subsidence accompanying groundwater extraction. *Hydrogeology Journal*, 19, 1459-1486.

Eguiluz de Antuñano, S., 2001, Geologic evolution and gas resources of the Sabinas Basin in northeastern Mexico. In Bartolini, C., Buffler, R.T., Cantú-Chapa, A., (eds.), The western Gulf of Mexico Basin: Tectonics, sedimentary basins, and petroleum systems. *AAPG Memoir*, 75, 241-270.

González-Sánchez, F., Puente-Solís, R., González-Partida, E., Camprubí, A., 2007, Estratigrafía del Noreste de México y su relación con los yacimientos estratoligados de fluorita, barita, celestina y Zn-Pb. *Boletín de la Sociedad Geológica Mexicana,* 59, 43-62.

Huebner, K.H., Thornton, E.A., 1995, The finite element method for engineers, John Wiley and Sons.

Hunt, K., Bigby, D., 1999, Designing for success. *World Coal*, 8(7), 47–52.

Martínez-López, J., Rey, J., Sandoval, S., Rodríguez, M., 2007, Electrical resistivity tomography: a tool to aid in the detection of mining voids (Arrayanes mine, Linares-Jaén). *Geogaceta*, 42, 43-46.

Militzer, H., Rösler, R., Lösch, W., 1979, Theoretical and experimental investigations for cavity research with geoelectrical resistivity methods. *Geophysical Prospecting*, 27, 640–652.

Peng, S., 2008, Coal Mine Ground Control, Third Edition. 764 pp.

Putiska, R., Nikolaj, M., Dostal, I., Kusnirak, D., 2012, Determination of cavities using electrical resistivity tomography. *Contributions to Geophysical and Geodesy*, 42, 201-211.

Rivera-Martínez, J. C., Alcocer-Valdés, C., 2003, La situación actual del aprovechamiento del carbón en el estado de Coahuila. *Boletín* Técnico de*l Consejo de Recursos Minerales*, 9, 2-19.

Secretaria de Economía (SE), 2017, Perfil del mercado del carbón. Coordinación General de Minería. Dirección General del Desarrollo Minero. Secretaría de Economía, México. 44 pp. https://www.gob.mx/cms/uploads/attachment/file/287796/Perfil_Carbon__2017.pdf.

Serrano-González, E., 2014, Identificación de riesgos geológicos ocasionados por la minería subterránea del carbón, en la cercanía de la Colonia Maseca, a partir de mediciones geoeléctricas. Tesis de licenciatura. Universidad Autónoma de Coahuila. 85 pp.

Servicio Geológico Mexicano (SGM), 2003, Carta geológico-minera Nueva Rosita G14-A13. Coahuila. Escala 1:50,000.

Strozik, G., Jendrus, R., Manowska, A., Popczyk, M., 2016, Mine Subsidence as a Post-Mining Effect in the Upper Silesia Coal Basin. *Pol. J. Environ. Stud*, 25(2), 777-785.

Thomas, L., 2013, Coal geology. Second edition. John Wiley & Sons. 444 pp.

Van der Merwe, J.N., Madden, B.J., 2010, Rock engineering of underground coal mining. Second edition. The Southern African Institute of Mining and Metallurgy. 259 pp.

Van Schoor, M., 2002, Detection of sinkholes using 2D electrical resistivity imaging. *Journal of Applied Geophysics*, 50, 393-399.

Ward, C.R., 1984, Coal Geology and Coal Technology. Blackwell Scientific Publications, Oxford, 345 pp.

Zhou, W., Beck, B.F., Adams, A.L., 2002, Effective electrode array in mapping karst hazards in electrical resistivity tomography. *Environ. Geol.*, 42, 922-928.